AIAA JOURNAL
Vol. 39, No. 11, November 2001

Initial Relaxation of Spatially Evolving Turbulent Channel Flow with Blowing and Suction

Yongmann M. Chung*
University of London, London, England E1 4NS, United Kingdom
and
Hyung Jin Sung†
Korea Advanced Institute of Science and Technology, Taejon 305-701, Republic of Korea

A direct numerical simulation is performed to examine the initial relaxation of spatially evolving turbulent channel flow subjected to uniform wall blowing and suction. Just beyond the entrance section, a uniform blowing is applied at the lower wall and a uniform suction at the upper. The relaxation processes of the mean velocity, turbulence intensities, Reynolds shear stresses, and vorticity fluctuations after the sudden wall blowing and suction are scrutinized. The effect of wall blowing and suction on the location and strength of the streamwise vortices is significant. The relaxation associated with suction is much slower than that with blowing. The initial relaxation is evaluated in terms of the turbulent kinetic energy transport. Blowing enhances the intercomponent energy transfer between the Reynolds stresses, whereas suction suppresses it.

I. Introduction

WHEN a fully developed turbulent wall-bounded flow is subjected to a step change in wall boundary conditions, there is an initial relaxation toward an equilibrium state after the step change of perturbation.[1,2] The perturbations can consist of, for example, wall blowing and suction, transverse pressure gradient, streamwise curvature, wall roughness, or wall temperature variation, etc. Among other perturbations, of major interest to the present study is the initial relaxation after the imposition of uniform wall blowing and suction. Wall blowing and suction have been encountered in many engineering problems such as turbine-blade cooling, transition delay, and separation prevention.[3–5]

Most previous studies of wall blowing and suction have concentrated on asymptotic cases. For these studies, uniform blowing and suction was applied for a long distance and the effects on the flow were investigated after the initial relaxation. Examples of this type of study are the experimental investigations of Antonia et al.,[3] Fulachier et al.,[4] the direct numerical simulation (DNS) of Sumitani and Kasagi,[6] and the large eddy simulation of Piomelli et al.[7] A DNS for a turbulent boundary layer with uniform suction is performed by Mariani et al.[8]

Although the effect of asymptotic wall blowing and suction on turbulence is well documented, studies on the initial relaxation after the wall blowing and suction are relatively scarce.[9,10] An experiment on a turbulent boundary layer subjected to a sudden increase in the wall blowing rate is performed by Simpson.[9] He reports the skin-friction coefficient and the mean velocity variations caused by an increased blowing rate, but details on the turbulent quantities are not available from the experiment. The extent to which previous studies have been performed has established that the flow cannot attain an equilibrium state immediately after wall blowing and suction. In the recovery process it is known that the first-order statistics such as the mean flow relax first and the second-order statistics such as the Reynolds stresses relax next.

The present study aims to depict the initial relaxation of a turbulent channel flow after wall blowing and suction. A fully developed turbulent channel flow is subjected to a sudden uniform wall blowing and suction immediately upon its exit from an entrance section. Figure 1 gives a schematic diagram of the flow configuration. The turbulence is perturbed from its equilibrium state and then allowed to reach another. An understanding of the initial relaxation is of prime importance in analyzing the effects of wall blowing and suction through a spanwise slot, where the wall blowing and suction is applied over a limited spatial extent rather than uniformly in space.[11–14] If the slot width is shorter than the length scale required for the initial relaxation, the flow cannot attain an asymptotic state. In general, the effects of local wall blowing and suction on the flow depend on the streamwise extent of the slot as well as the strength of the blowing and suction and consequently on the characteristics of the initial relaxation.

Received 9 August 2000; revision received 14 March 2001; accepted for publication 14 March 2001.

*Postdoctoral Researcher, Department of Engineering, Queen Mary; currently Postdoctoral Researcher, Department of Engineering, University of Warwick, Coventry, England CV4 7AL, United Kingdom.

†Professor, Department of Mechanical Engineering, 373-1 Kusong-dong, Yusong-ku; hjsung@kaist.ac.kr.

II. Numerical Method

A. Governing Equations

For an incompressible flow, the unsteady three-dimensional Navier–Stokes and continuity equations can be written in the following nondimensional form:

$$\frac{\partial u_i}{\partial t} + \frac{\partial}{\partial x_j}(u_i u_j) = -\frac{\partial p}{\partial x_i} + \frac{1}{Re}\frac{\partial^2 u_i}{\partial x_j \partial x_j} \tag{1}$$

$$\frac{\partial u_i}{\partial x_i} = 0 \tag{2}$$

where u_i is the instantaneous velocity in the x_i direction and p is the pressure. The instantaneous velocity is decomposed into $u_i = U_i + u_i'$, where U_i is the time-mean velocity and u_i' is the fluctuating velocity component. The subscripts i, j, k take values of 1, 2, 3 to denote the streamwise x, normal to the wall y, and spanwise z directions, respectively. All flow variables are nondimensionalized by the inlet bulk mean velocity U_m and the channel half-width h. The Reynolds number is defined as $Re = U_m h/\nu$, where ν is the kinematic viscosity of the fluid.

The numerical method used for this study was originally developed by Yang and Ferziger.[15] Here, we only summarize the numerical method briefly. Details regarding the procedures can be found in Yang and Ferziger[15] and Chung and Sung.[16] The governing equations are discretized on a staggered grid. They are integrated in time using a fractional-step method,[15,17] based on a time-splitting method in conjunction with the approximate factorization technique. The solution procedure consists of a semi-implicit approach. It uses a low storage, third-order Runge–Kutta method for the nonlinear convective terms and a second-order Crank–Nicholson method for the viscous terms. For spatial discretization, second-order central differences are used. The Poisson equation for pressure is solved in the wave-number space by Fourier transformation in the streamwise

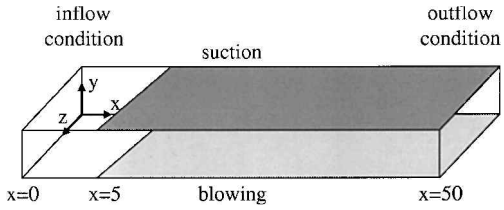

Fig. 1 Schematic diagram of flow configuration.

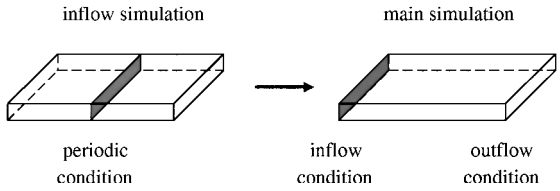

Fig. 2 Inflow simulation.

and spanwise directions, taking advantage of the uniform grid spacings in those directions. The code has been used for transitional[18] and turbulent flows.[15,16]

B. Boundary Conditions

In the present study, uniform wall blowing and suction are applied from $x = 5$ to the exit of the computational domain. A uniform blowing is imposed at the lower wall and a uniform suction at the upper wall (see Fig. 1). The rates of blowing and suction set equal. This boundary condition implies that the net mass flux associated with the blowing and suction is zero and that the bulk mean velocity is constant through the computational domain. At the wall, no-slip boundary conditions are imposed. The vertical component v is zero at $x \leq 5$ and $v = v_0$ at $x > 5$.

At the outflow boundary, the convective boundary condition[19] is applied

$$\frac{\partial u_i}{\partial t} + U_c \frac{\partial u_i}{\partial x} = 0 \tag{3}$$

where U_c is the convective velocity at the exit. In this study U_c is equal to the bulk mean velocity at the inlet U_m. Periodic boundary conditions are employed in the spanwise direction.

C. Inflow Simulation

Implementation of a proper inflow condition is important to simulate spatially evolving turbulent flows.[16] To impose a real turbulence at the inflow boundary, an auxiliary periodic DNS of a fully developed turbulent channel flow is performed concurrently with the main simulation. As sketched in Fig. 2, the instantaneous velocity field obtained from the inflow simulation on a plane perpendicular to the streamwise direction is imposed at each time step.[16] It is known that the inflow data taken from an auxiliary inflow simulation can supply an ideal inflow condition to a spatially evolving simulation. The main advantage of this inflow condition is that it can provide an unsteady turbulence inflow with correct phase information and dynamics. Thus, the dynamic characteristics of flow structure, such as the low-speed streaks, can be portrayed. However, in other synthetic boundary conditions, the correct near-wall behavior of each component of the Reynolds stresses could not be obtained.

The inflow simulation is matched to ensure that the meshing in all three directions and the time step are identical to the main simulation. The streamwise and spanwise dimensions of the inflow simulation are $12.8h$ and $3h$, respectively. A $128 \times 129 \times 64$ grid system is used to obtain identical grid spacings compared to the main simulation.

D. Numerical Parameters

In the present study $Re = 2.18 \times 10^3$, which corresponds to $Re_\tau = 1.5 \times 10^2$ based on the wall friction velocity at inlet $u_{\tau_{\text{in}}}$. Here, u_τ is defined as $\sqrt{(\tau_w/\rho)}$, where $\tau_w = \mu(dU/dy)$ is the wall shear stress and ρ is the density of the fluid. The dimensionless wall transpiration velocity $v_0^+ (= v_0/u_{\tau_{\text{in}}})$ is set to be 0.05, which corresponds to a wall transpiration rate $v_0/U_m = 0.00344$. The transpiration velocity is the same as used by Sumitani and Kasagi.[6]

The computational domain size and the grid resolutions are chosen through preliminary simulations.[11,12,20] The streamwise and spanwise dimensions of the computational domain are set to $L_x = 51.2h$ and $L_z = 3h$, respectively. So as to describe the initial relaxation process after the perturbation, the box length in the streamwise direction is made large. The spanwise autocorrelation decays to zero. This suggests that the box size is sufficiently large in the spanwise direction.

Grid refinement is performed until more grid points do not cause any significant differences in the result.[20] A $512 \times 129 \times 64$ grid system is used in the x, y, and z directions, respectively. To resolve the near-wall structure, grid stretching is implemented along the wall-normal direction y using a hyperbolic tangent distribution. The first grid point away from the wall is located at about $y^+ \approx 0.1$. The streamwise and spanwise grid resolutions are $\Delta x^+ = 15.0$ and $\Delta z^+ = 6.25$, respectively. Effects of computational time step are investigated by successively halving the time step. The time step used is $\Delta t = 0.02(\Delta \tilde{t} U_m/h)$, i.e., $\Delta t^+ = 0.2\Delta \tilde{t} u_\tau^2/\nu$ in wall units, where $\tilde{t}$ is the dimensiional time. After a transient period converged time-mean quantities are obtained for $12{,}000\Delta t$, which corresponds to $240(\tilde{t}U_m/h)$ or $2400\,\tilde{t}u_\tau^2/\nu$ in wall units.

III. Results and Discussion

A. Instantaneous Flowfield

To gain a better understanding of the initial relaxation, instantaneous flowfields are displayed. Figure 3 gives contours of three components of instantaneous velocity at midspan in the x–y plane. The time-mean velocity is not subtracted from the instantaneous velocity. The y coordinate is enlarged by a factor of four giving a more detailed picture near the wall. A global inspection of the flow changes after the uniform blowing and suction ($x > 5$) reveals that the turbulent motions are energetic in the lower wall. However, the near-wall turbulent motions are suppressed for the upper wall. The influence of blowing and suction is more distinctly shown in the transverse components. It is seen in Fig. 3a that the formation of a shear layer, with a locally high velocity gradient, in the vicinity of the upper wall is significantly suppressed. On the suction side, there are few inflections in the instantaneous streamwise velocity profiles. This is indicative of suppression of the near-wall turbulent bursts. These observations are consistent with the experimental findings.[21]

The instantaneous streamwise velocity fluctuations at $y^+ = 5$ in the x–z plane are exhibited in Fig. 4. The low-speed streaks are elongated substantially on the suction wall; in particular, some streaks are as long as $\lambda_x^+ = 2000$ (Ref. 3). The elongated streaks imply an increased mean period of the bursting near the suction wall,[21] causing a weakening of the downstream turbulence. The meanderings of the low-speed streaks are significantly weakened because of the reduced transverse motion.

B. Coefficient of Friction and Pressure

The wall skin-friction coefficient C_f, which is defined as $C_f = \tau_w/\frac{1}{2}\rho U_m^2$, is normalized by the inlet velocity U_m. The initial relaxation process with uniform blowing can be divided into four regions as shown in Fig. 5. In region I ($5 < x < 8$), C_f decreases sharply after the application of blowing. Consequently, large variations of V in the wall-normal direction are produced (see Fig. 6b). In region II ($8 < x < 18$), C_f on the blowing wall increases slightly to a local maximum. The flow characteristics in region III ($8 < x < 32$) show a very small decrease in C_f. In region IV, extending downstream from $x > 32$, C_f on the blowing wall has almost a constant value. The overshoot of C_f in region I indicates that the early response of C_f seems to be less related to the turbulent flow structure. It appears that the later adjustment observed in regions II and III is associated with the turbulent coherent structure modification. The early response of C_f with uniform suction in region I shows a similar behavior to that of the blowing case. However, C_f on the suction wall does not reach a fully developed state until the exit of the computational domain, showing a slower relaxation with suction.

The pressure coefficient C_p is defined by $C_p = (p - p_{\text{in}})/\frac{1}{2}\rho U_m^2$, where p_{in} is a reference inlet pressure. The streamwise variations of C_p are represented in Fig. 7. Except for region I (see Fig. 5) where the pressure gradient changes from adverse to favorable with

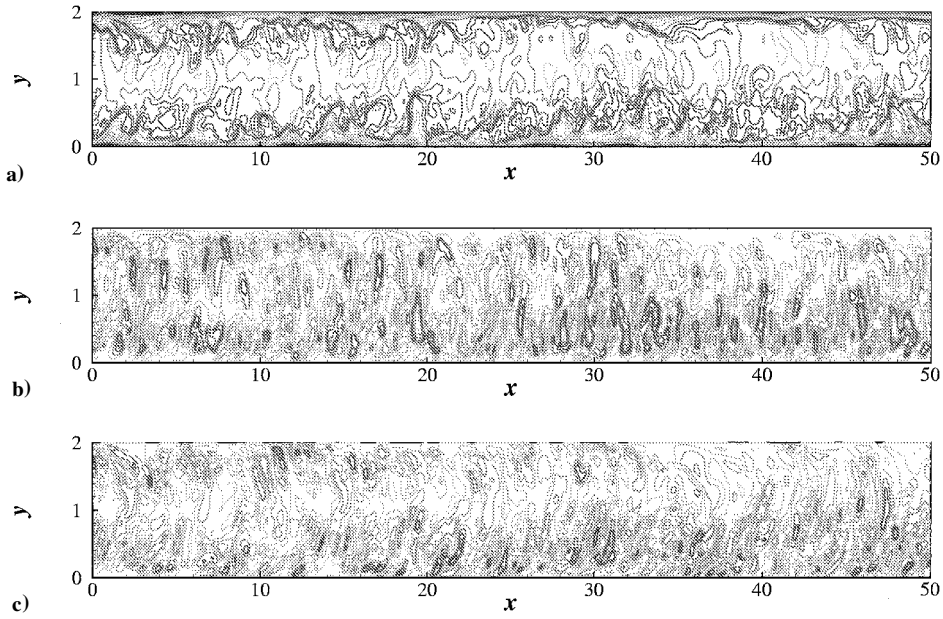

Fig. 3 Contours of instantaneous velocity components in the x–y plane: a) $U+u$, b) $V+v$, and c) w. Contour lines for u are from 0.0 to 1.23 with increments of 0.082, v from −0.189 to 0.177 with increments of 0.026, and w from −0.286 to 0.291 with increments of 0.041.

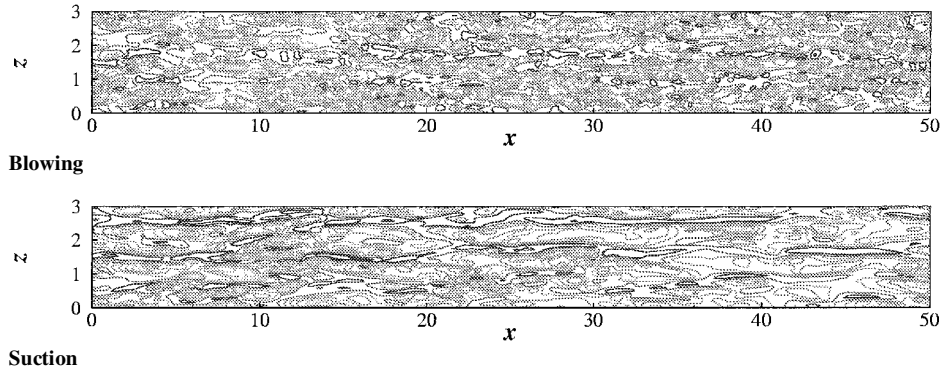

Fig. 4 Contours of instantaneous streamwise velocity fluctuations in the x–z plane.

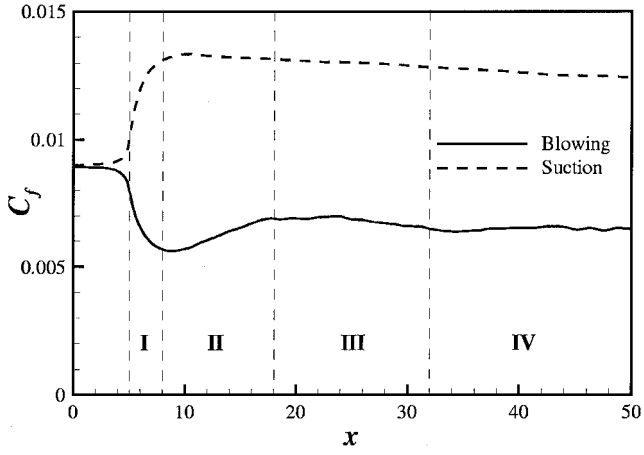

Fig. 5 Streamwise variations of the skin-friction coefficient C_f.

blowing and favorable to adverse with suction, C_p has almost a constant gradient. This suggests that in this case the wall pressure is not as sensitive as C_f to the downstream flow development.

C. Mean Velocity

Figure 6 plots mean velocities at six streamwise locations. The periodic DNS results of the unperturbed turbulent channel flow[22] and the asymptotic wall blowing and suction[6] are included for comparison. At the inflow region, the streamwise velocity shows good agreement with the periodic DNS.[22] After the application of blowing and suction, the core region has a slow response to the wall blowing and suction. However, the time-mean velocity near the wall adjusts quickly to the perturbation (see Fig. 5). Near the exit the general features of the velocity profile are consistent with those of the periodic DNS.[6] For $0 < y < 0.3$, the profile at $x = 45$ is in agreement with periodic DNS data,[6] whereas the suction profile deviates substantially from the periodic DNS, showing a slow response to the wall suction.

For the early stage of initial relaxation ($x = 6$ and 13), $\partial U/\partial x < 0$ in the lower part of the channel ($0 < y < 0.5$) and $\partial U/\partial x > 0$ in the upper part ($1.5 < y < 2$). Consequently, because of continuity, $\partial V/\partial y$ should be positive in the lower part of the channel and negative in the upper part. Away from both walls, the normal velocity V increases from the wall transpiration velocity v_0 and is nearly uniform across the channel. Just after the wall blowing and suction, V has a maximum, i.e., $V = 3v_0$ at $x = 6$.

To examine the near-wall behavior, the streamwise velocity profiles are illustrated in terms of $u^+ = \tilde{U}/u_\tau$ and $y^+ = \tilde{y}u_\tau/\nu$ (where $U = \tilde{U}/U_m$ and $y = \tilde{y}/h$). Here, the local friction velocity u_τ is calculated along the streamwise direction at each wall. Figure 8 shows the logarithmic velocity profiles at several representative downstream locations, together with DNS data.[6,22] As seen in prior experimental and numerical studies,[6,7] an upward shift of the logarithmic velocity profile caused by blowing and a downward shift by suction are clearly displayed.

A fast initial relaxation with blowing is observed in Fig. 8, which is in accord with the finding for the C_f distribution. For blowing, the

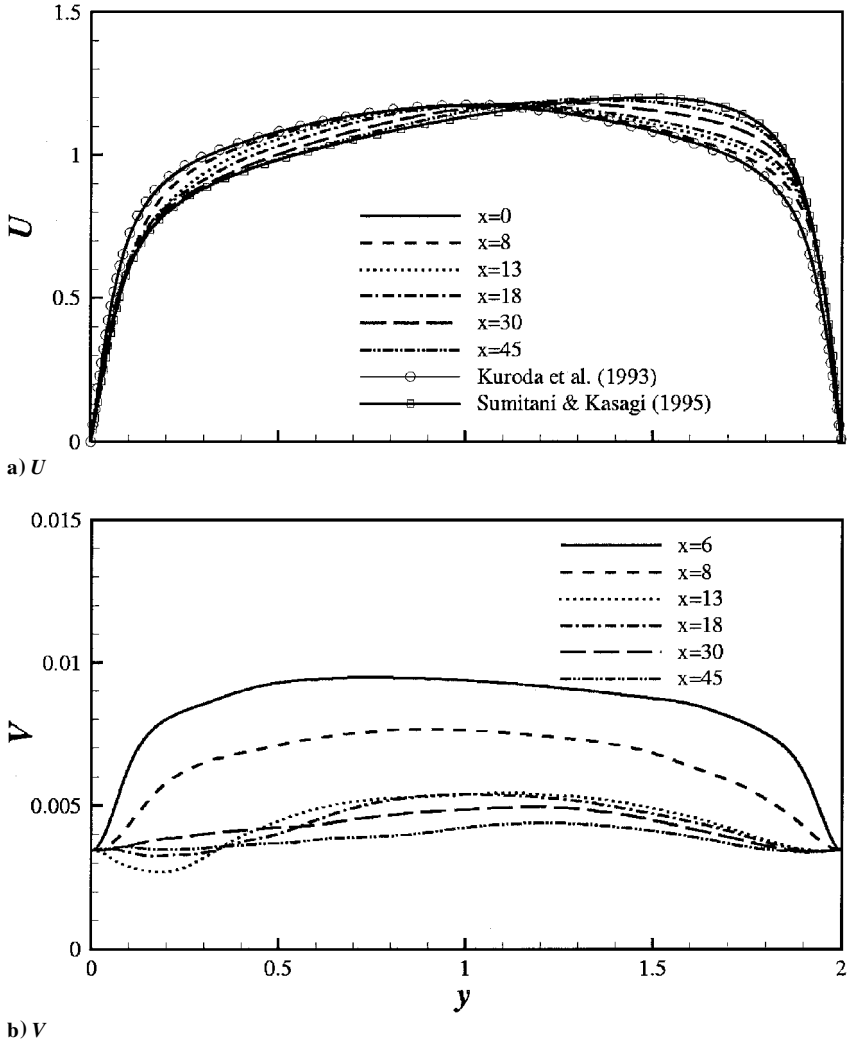

Fig. 6 Profiles of time mean velocity components at several streamwise locations.

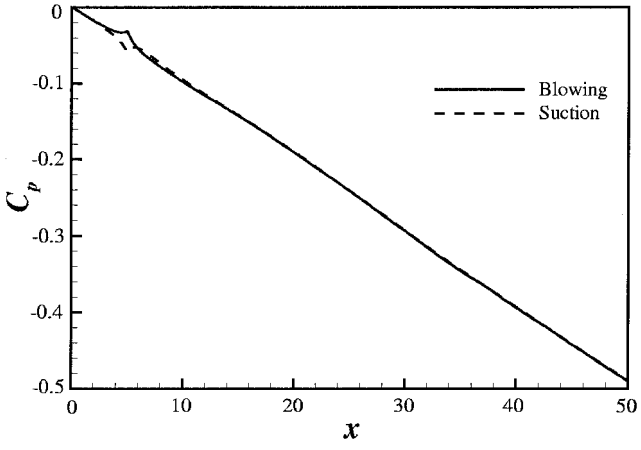

Fig. 7 Streamwise variations of the pressure coefficient C_p.

velocity profile attains almost its fully developed state as early as at $x = 18$. In the case of suction, it is not until the furthest downstream location that the profiles approach the periodic simulation data. Near the exit the logarithmic velocities show good agreement with the periodic DNS.[6]

D. Turbulence Intensities and Reynolds Stresses

Figure 9 gives contours of the turbulence intensities ($\overline{u'^2}$, $\overline{v'^2}$, and $\overline{w'^2}$) and the Reynolds shear stress ($-\overline{u'v'}$). As seen, blowing and suction significantly modify the turbulence intensities. It is evident that the former enhances turbulence and the latter suppresses it. The blowing side response is faster than that for the suction side. After the wall blowing the turbulence intensities have an increased near-wall peak. Farther downstream, the turbulence intensities on the blowing side reach an equilibrium state in region III, while turbulence intensities on the suction side keep decreasing to the exit of the computational domain. The response of each turbulence intensity component to the wall perturbation is seen to be different. The streamwise component shows the quickest response.

Streamwise variations of the maxima in the Reynolds stresses ($\overline{u'^2}$, $\overline{v'^2}$, $\overline{w'^2}$, and $-\overline{u'v'}$) with blowing and suction are displayed in Fig. 10. When suction is applied, $\overline{v'^2}$ and $\overline{w'^2}$ have a broad peak (see Fig. 11) indicating that the local maximum in the suction side is not distinctive. To avoid any ambiguity, therefore, the $\overline{v'^2}$ and $\overline{w'^2}$ data on the suction side are the values at $y = 1.7$, corresponding to the location for the maximum values without blowing and suction. For convenience to match the magnitudes, values multiplied by four for $\overline{v'^2}$, $\overline{w'^2}$, and $-\overline{u'v'}$ are shown.

When blowing is applied, $\overline{u'^2}$ increases, having a maximum value at $x = 13$. It then decreases to its inflow value. The responses of $\overline{v'^2}$ and $\overline{w'^2}$ are slower than that of $\overline{u'^2}$. It is seen that $\overline{v'^2}$ reaches a maximum at about $x = 20$ and $\overline{w'^2}$ at around $x = 16$. In the case of suction, relaxation is much slower. There is no sign of attaining an equilibrium state until the exit of the computational domain.

The influence of wall blowing and suction on the transverse component is larger than on the streamwise component. Blowing enhances $\overline{v'^2}$ and $\overline{w'^2}$ more significantly than $\overline{u'^2}$. The increase of $\overline{u'^2}$ after blowing is almost negligible although it has a maximum

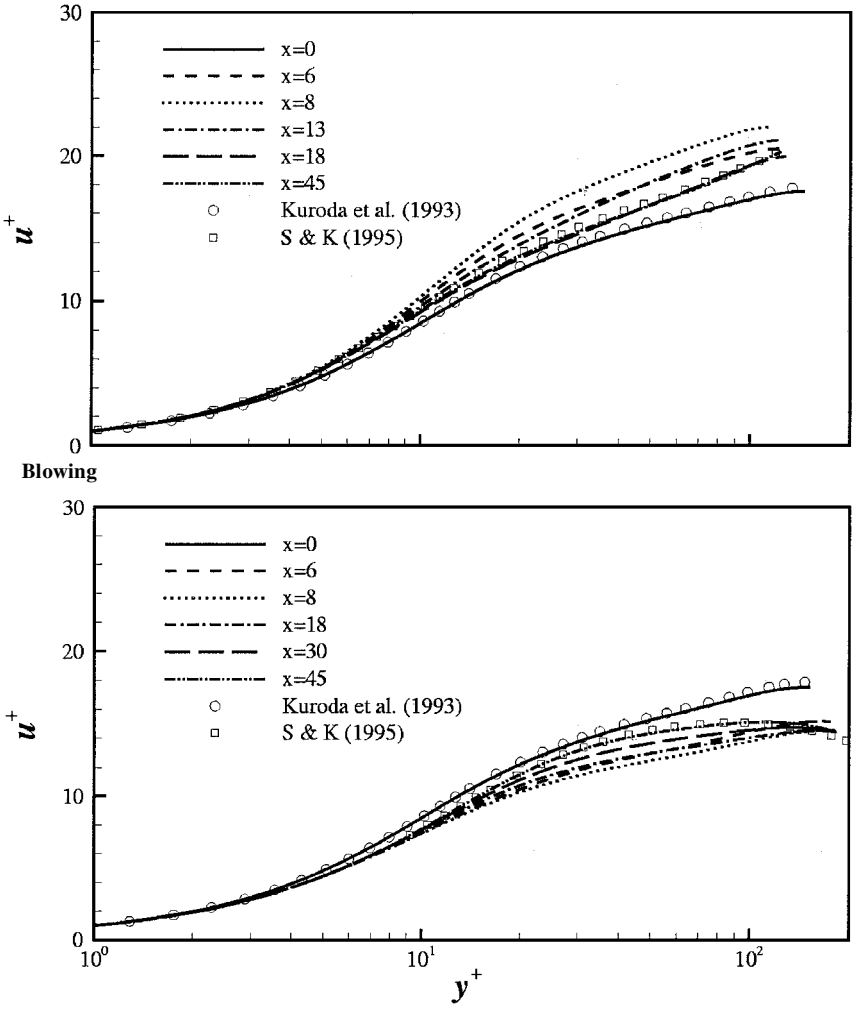

Fig. 8 Mean streamwise velocity profiles in wall coordinates at several streamwise locations.

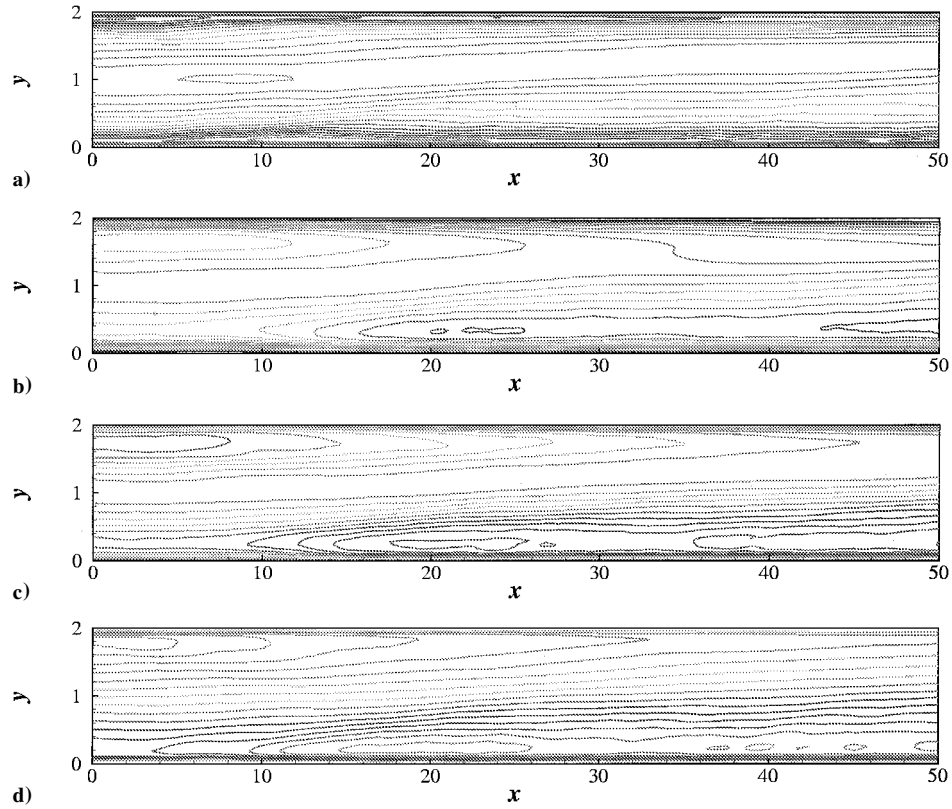

Fig. 9 Contours of turbulence intensities: a) u', b) v', c) w', and d) $-\overline{u'v'}$. The increments for u' are 0.01 and 0.005 elsewhere.

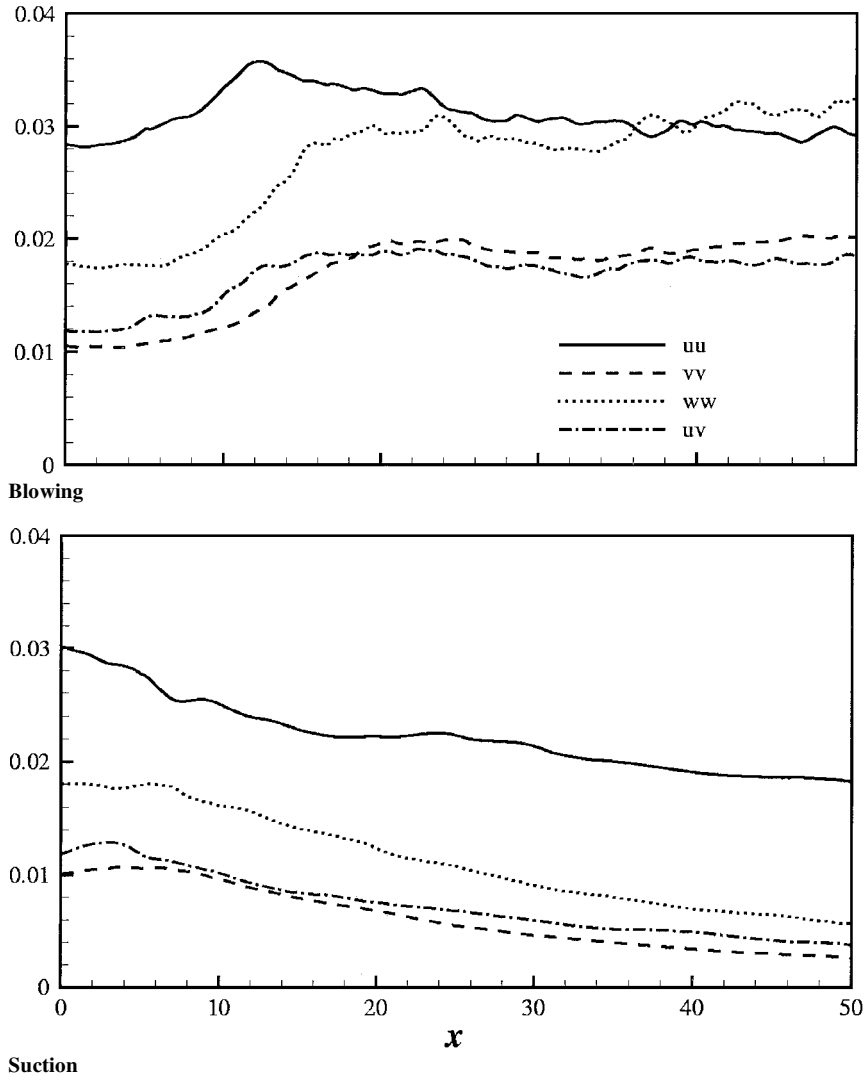

Fig. 10 Streamwise variations of the Reynolds stresses ($\overline{u'^2}$, $4\overline{v'^2}$, $4\overline{w'^2}$, and $-4\overline{u'v'}$).

increase of 30% at $x = 13$, whereas $\overline{v'^2}$ and $\overline{w'^2}$ are increased by 90%. Consequently, blowing plays a role in returning to isotropy. In the upper wall, suction weakens the transverse motion rather than the streamwise motion. The reduction rate of $\overline{u'^2}$ by suction is about 35%, whereas $\overline{v'^2}$ and $\overline{w'^2}$ are about 70 and 80%, respectively.

Comparison is extended to the Reynolds-stress anisotropy tensor $b_{ij} = \overline{u'_i u'_j}/2k - \delta_{ij}/3$ and its second invariant $II = -\frac{1}{2} b_{ij} b_{ji}$ (not shown here). Just after the application of wall blowing, an immediate increase of the anisotropy is observed as a result of the earlier increase of $\overline{u'^2}$ in region I (Figs. 9 and 10). As $\overline{v'^2}$ and $\overline{w'^2}$ increases, anisotropy decreases in region II. Farther downstream in regions III and IV, it is likely that the flow anisotropy on the blowing side approaches an equilibrium state along with the Reynolds stresses. On the suction case the anisotropy increases slowly with a small decrease after the application of the suction. This is attributed to the earlier response of $\overline{u'^2}$ to the application of suction. The enhanced anisotropy in the wall region with suction is also found in the experiment of Antonia et al.[3] and DNS boundary-layer flow data.[5,8]

Figure 11 gives the near-exit turbulence intensity profile. An increase with blowing and a decrease with suction are clearly seen. As mentioned earlier, v' and w' increase substantially on the blowing side although u' has almost the same magnitude as the inflow value. Where v' and w' are influenced more than u', turbulence is suppressed enhancing anisotropy. Because of the variations of u_τ shown in Fig. 12, when nondimensionalized by wall variables, changes in turbulence intensities are amplified.

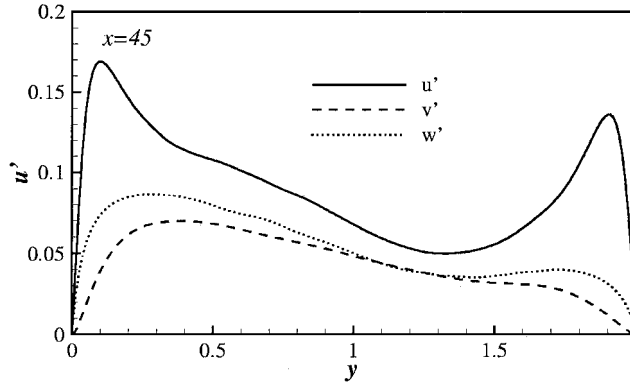

Fig. 11 Profiles of turbulence intensities at $x = 45$.

E. Vorticity Fluctuations

Contours of the three components of the vorticity fluctuations ($\omega_i = \sqrt{\omega_i'^2}$) are analyzed but because of space limits not shown here. Comparing with Fig. 9, the response of ω_x is similar to those of v' and w'. The strength of v' and w' increases to $10h$ downstream after the application of wall blowing. On the contrary, ω_y has an immediate response to the wall blowing and suction. Because the streamwise vortices are closely related to the near-wall turbulent activities, the response of the near-wall turbulent flow to blowing and suction can be explained in terms of the streamwise vortices. The location of the local maximum ω_x corresponds to the average

location of the center of the streamwise vortices. The average size of the streamwise vortex can be estimated from the distance between the local maximum and minimum.[23]

Figure 13 shows the variation of the maximum values of vorticity fluctuations. In region I, as blowing is applied, the streamwise vortices move away from the wall while the strength of the streamwise vortices does not adjust to the new environment, having the same value. At the same time the wall value of ω_x experiences a sharp drop after the application of wall blowing. Because of the no-slip boundary condition, the streamwise vorticity with opposite sign is created at the wall. The response of the wall value of ω_x is immediate upon the application of the wall perturbation. In region II the strength of the streamwise vortices increases up to 40%. Subsequently, the wall value of ω_x also increases. In region III the strength of the streamwise vortices reaches a fully developed state, which is consistent with the findings in the Reynolds stress shown in Fig. 10.

In the suction wall at region I the response of ω_x is significant. Further downstream from region II, all of the vorticity fluctuations gradually decrease until the exit of the computational domain. Although the decreases are small, they never attain a fully developed value again.

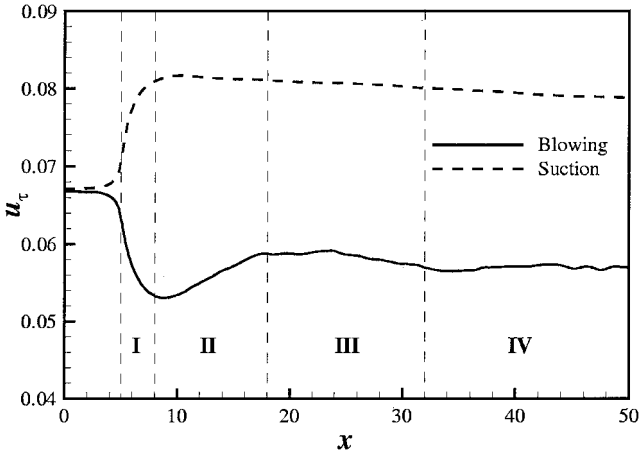

Fig. 12 Streamwise variations of the friction velocity u_τ.

F. Turbulent Kinetic Energy Budget

The transport equations for Reynolds stress can provide more information on the underlying physics of near-wall turbulence transport. For an incompressible turbulent flow the Reynolds-stress transport equations are given by

$$\frac{\partial \overline{u_i u_j}}{\partial t} + C_{ij} = P_{ij} + T_{ij} + \Pi_{ij} + \Phi_{ij} + D_{ij} + \epsilon_{ij} \tag{4}$$

Here

$$C_{ij} = U_k \frac{\partial}{\partial x_k}\overline{u_i u_j}, \qquad P_{ij} = -\left(\overline{u_i u_k}\frac{\partial U_j}{\partial x_k} + \overline{u_j u_k}\frac{\partial U_i}{\partial x_k}\right)$$

$$T_{ij} = -\frac{\partial}{\partial x_k}\overline{u_i u_j u_k}, \qquad \Pi_{ij} = -\frac{1}{\rho}\left(\frac{\partial}{\partial x_i}\overline{p u_j} + \frac{\partial}{\partial x_j}\overline{p u_i}\right)$$

$$\Phi_{ij} = \overline{\frac{1}{\rho} p\left(\frac{\partial u_i}{\partial x_j} + \frac{\partial u_j}{\partial x_i}\right)}, \qquad D_{ij} = \nu \frac{\partial^2}{\partial x_k^2}\overline{u_i u_j}$$

$$\epsilon_{ij} = -2\nu \overline{\frac{\partial u_i}{\partial x_k}\frac{\partial u_j}{\partial x_k}}$$

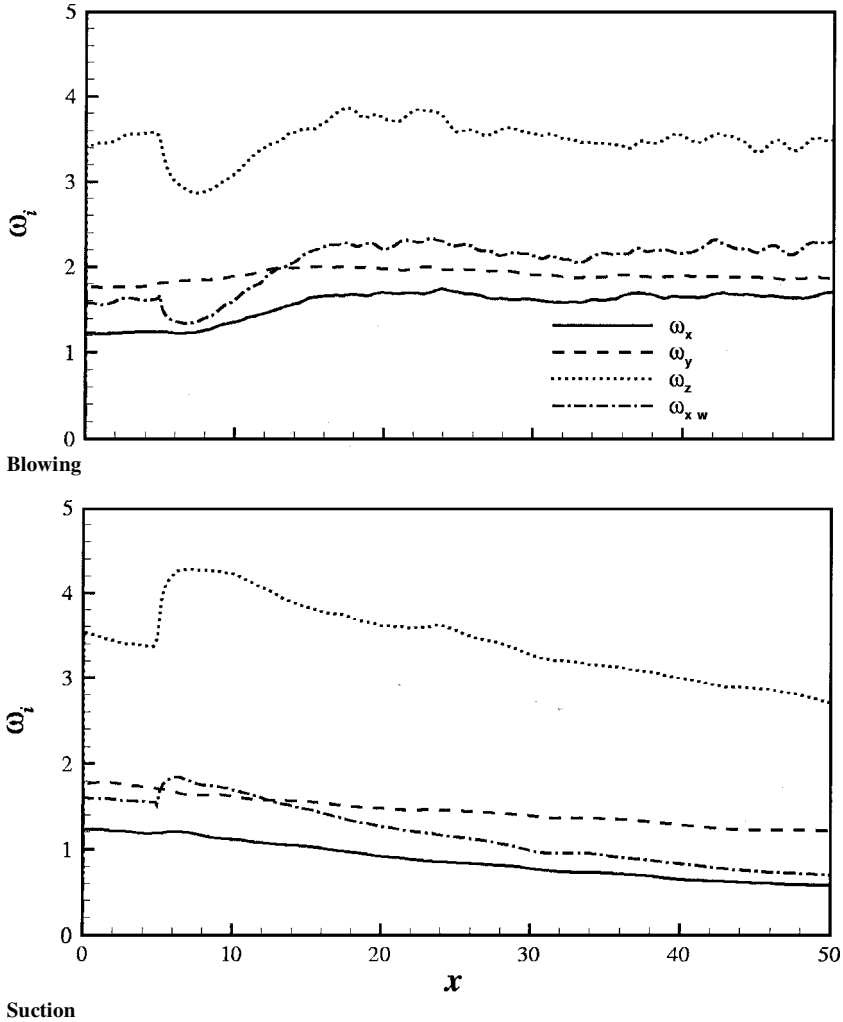

Fig. 13 Maximum values of vorticity fluctuations.

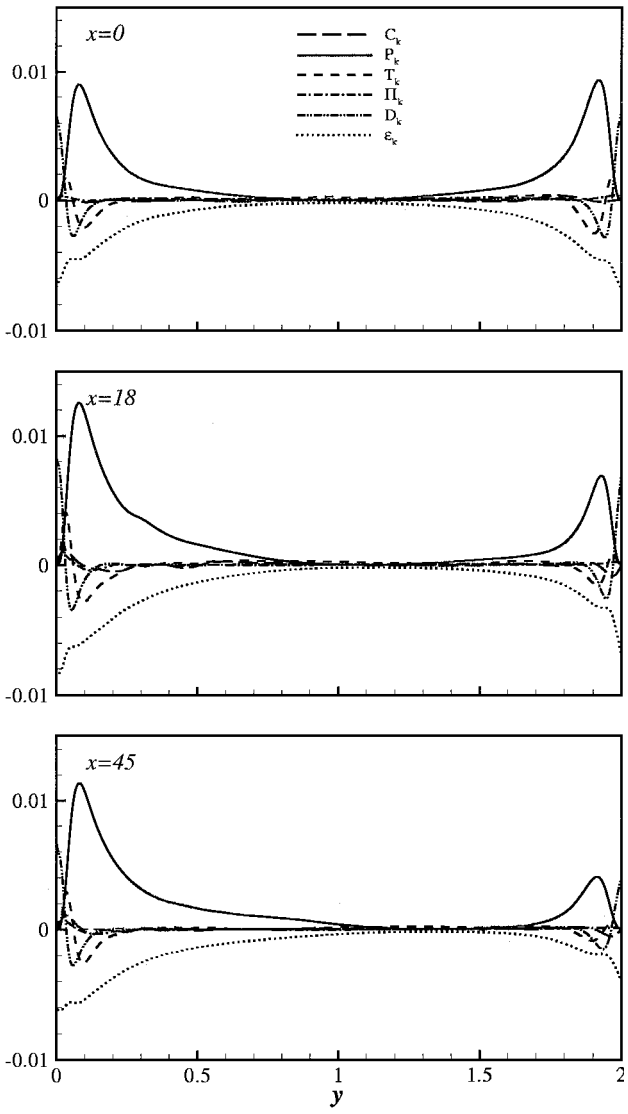

Fig. 14 Budget of k.

where C_{ij}, P_{ij}, T_{ij}, Π_{ij}, Φ_{ij}, D_{ij}, and ϵ_{ij} denote the convection, production, turbulent transport, pressure transport, pressure-strain correlation, viscous diffusion and viscous dissipation, respectively. In other studies the sum of Π_{ij} and Φ_{ij} is referred to as the velocity-pressure gradient term.[24]

The budget of these terms is shown in Fig. 14 at four streamwise locations. The location $x = 18$ is the end of region II. The location $x = 45$ is close to the end of the computational domain (see Fig. 5). The budget terms are normalized by U_m^3/h. The budget at the inflow agrees well with that of periodic DNS.[22,24] In region I ($5 < x < 8$) blowing significantly increases P_k, T_k, and Π_{ij}, whereas D_k and ϵ_k experience a sharp near-wall decrease. At $x = 8$ the wall values of D_k and ϵ_k have a minimum. In region II all of the budget terms including D_k and ϵ_k increase, having a maximum at $x = 18$, followed by a slight decrease in region III. In region IV there is little change in the budget. This suggests that near the blowing wall an equilibrium state is achieved.

As suction is applied, D_k and ϵ_k increase sharply in region I, having a maximum at $x = 8$. From region II all of the budget terms decrease monotonically until the exit of the computational domain. The budget in the blowing side at $x = 18$ and 45 is not changed significantly. However, it decreases by half in the suction case, showing a much more rapid response of flow to blowing. Near the exit (Fig. 14d), the budget on each side is qualitatively similar. However, magnitudes are much different. The magnitude of each term in the blowing side is increased by 30%, while the reduction in the suction side is about 60%. This means that the suction effect is substantial. When the budget terms are nondimensionalized using wall variables

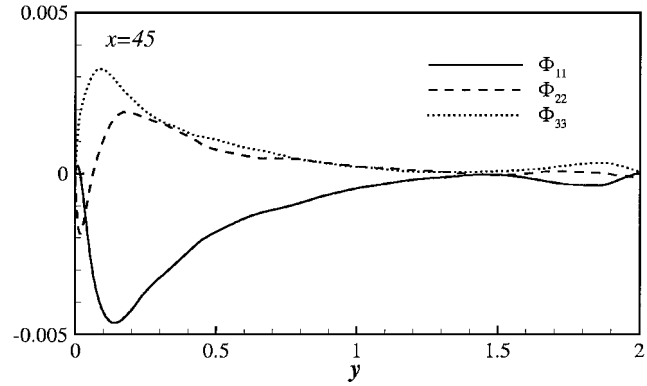

Fig. 15 Pressure-strain correlation term Φ_{ij} in the budget of k at $x = 45$.

(u_τ^4/ν) with the local friction velocity at each wall, the budget in the blowing case increases 2.5 times. However, the magnitude in the suction side is reduced to only a quarter of its inflow value. In wall units the locations for the local maximum and minimum of the budget are also changed: it moves toward the wall in the blowing case, whereas the reverse occurs on the suction side. Again, the effect of u_τ in Fig. 12 is significant in the budget change.

To investigate the intercomponent energy transfer between the Reynolds-stress components, the pressure-strain correlation terms Φ_{ij} near the exit are represented in Fig. 15. In the budget of turbulent kinetic energy (see Fig. 14), there is no contribution from the pressure-strain correlation term. As the flow goes downstream, Φ_{ij} near the blowing wall approaches an equilibrium state in region II, whereas the relaxation is not completed in the suction case even near the exit. It is seen that the change in Φ_{ij} is more significant than for the other terms in the turbulence energy budget. On the blowing side Φ_{ij} is double the inflow value, while Φ_{ij} on the suction side is a quarter of this value. The turbulent kinetic energy budget shows a 30% increase on the blowing side and a 60% decrease on the suction side. Blowing enhances the intercomponent energy transfer substantially while suction prevents it. Consequently, blowing gives rise to much enhanced isotropy and suction the reverse.

IV. Conclusions

In the present study a direct numerical simulation is performed to scrutinize the effect of uniform wall blowing and suction on turbulent channel flow. A fully developed turbulent channel flow is subjected to sudden wall blowing and suction. The downstream evolutions of flow structure and the rate of adjustment to a new structure are evaluated. The initial relaxation after the wall blowing and suction is found to be slow. Because of the vertical momentum flux, immediately after blowing and suction (region I) the streamwise vortices move. Consequently, the time-mean velocity begins to change. However, the strength of the streamwise vortices is not adjusted until region II, where blowing intensifies the vortical motions and suction suppresses them. In this region all of the turbulent quantities are modified, including the anisotropy tensor and the Reynolds stresses. Farther downstream, with uniform blowing near-wall turbulence shows a quick response compared to the suction case. However, turbulence on the suction side never approaches an equilibrium state until the exit of the computational domain. On the blowing case all terms in the budget of turbulent kinetic energy k and vorticity fluctuation ω_x increase substantially, whereas with suction they decrease. It is found that blowing enhances intercomponent energy transfer between velocity fluctuations, while suction diminishes it. Consequently, anisotropy is much enhanced on the suction side.

Acknowledgments

This research was supported by a grant from the National Research Laboratory of the Ministry of Science and Technology, Republic of Korea. Computational resources for this work were provided by the Korea Research and Development Information Center. The authors are grateful to Kyung-Soo Yang for assistance with computational aspects of this work and for permitting us to use

his program. In addition, we thank Paul G. Tucker for reading the manuscript.

References

[1]Smits, A. J., and Wood, D. H., "The Response of Turbulent Boundary Layers to Sudden Perturbations," *Annual Review of Fluid Mechanics*, Vol. 17, 1985, pp. 321–358.

[2]Bushnell, D. M., and McGinley, C. B., "Turbulence Control in Wall Flows," *Annual Review of Fluid Mechanics*, Vol. 21, 1989, pp. 1–20.

[3]Antonia, R. A., Fulachier, L., Krishnamoorthy, L. V., Benabid, T., and Anselmet, F., "Influence of Wall Suction on the Organized Motion in a Turbulent Boundary Layer," *Journal of Fluid Mechanics*, Vol. 190, 1988, pp. 217–240.

[4]Fulachier, L., Anselmet, F., Benabid, T., and Antonia, R. A., "Normalization for a Turbulent Boundary Layer with Wall Suction," *Physics of Fluids A*, Vol. 3, No. 1, 1991, pp. 233–235.

[5]Antonia, R. A., Spalart, P. R., and Mariani, P., "Effect of Suction on the Near-Wall Anisotropy of a Turbulent Boundary Layer," *Physics of Fluids*, Vol. 6, No. 1, 1994, pp. 430–432.

[6]Sumitani, Y., and Kasagi, N., "Direct Numerical Simulation of Turbulent Transport with Uniform Wall Injection and Suction," *AIAA Journal*, Vol. 33, No. 7, 1995, pp. 1220–1228.

[7]Piomelli, U., Ferziger, J. H., and Moin, P., "New Approximate Boundary Conditions for Large Eddy Simulations of Wall-Bounded Flows," *Physics of Fluids A*, Vol. 1, No. 6, 1989, pp. 1061–1068.

[8]Mariani, P., Spalart, P. R., and Kollmann, W., "Direct Simulation of a Turbulent Boundary Layer with Suction," *Near-Wall Turbulent Flows*, edited by R. M. C. So, C. G. Speziale, and B. E. Launder, Elsevier, Amsterdam, 1993, pp. 347–356.

[9]Simpson, R. L., "The Effect of a Discontinuity in Wall Blowing on the Turbulent Incompressible Boundary Layer," *International Journal of Heat and Mass Transfer*, Vol. 14, 1971, pp. 2083–2097.

[10]Schildknecht, M., Miller, J. A., and Meier, G. E. A., "The Influence of Suction on the Structure of Turbulence in Fully Developed Pipe Flow," *Journal of Fluid Mechanics*, Vol. 90, 1979, pp. 67–107.

[11]Chung, Y. M., and Sung, H. J., "Effects of Local Blowing on Spatially-Evolving Turbulent Channel Flow," *Proceedings of the Fourth KSME–JSME Fluids Engineering Conference*, Pusan, Republic of Korea, 1998, pp. 673–676.

[12]Chung, Y. M., and Sung, H. J., "Asymmetric Response of Turbulent Channel Flow to Wall Suction and Blowing," *Proceedings of the First International Symposium on Turbulence and Shear Flow Phenomena*, edited by S. Banerjee and J. K. Eaton, Begell House, New York, 1999, pp. 423–428.

[13]Park, J., and Choi, H., "Effects of Uniform Blowing or Suction from a Spanwise Slot on a Turbulent Boundary Layer Flow," *Physics of Fluids*, Vol. 11, No. 10, 1999, pp. 3095–3105.

[14]Antonia, R. A., Zhu, Y., and Sokolov, M., "Effect of Concentrated Wall Suction on a Turbulent Boundary Layer," *Physics of Fluids*, Vol. 7, No. 10, 1995, pp. 2465–2474.

[15]Yang, K.-S., and Ferziger, J. H., "Large-Eddy Simulation of Turbulent Obstacle Flow Using a Dynamic Subgrid-Scale Model," *AIAA Journal*, Vol. 31, No. 8, 1993, pp. 1406–1413.

[16]Chung, Y. M., and Sung, H. J., "Comparative Study of Inflow Conditions for Spatially Evolving Simulation," *AIAA Journal*, Vol. 35, No. 2, 1997, pp. 269– 274.

[17]Kim, J., and Moin, P., "Application of a Fractional-Step Method to Incompressible Navier–Stokes Equations," *Journal of Computational Physics*, Vol. 59, No. 2, 1985, pp. 308–323.

[18]Chung, Y. M., Sung, H. J., and Boiko, A. V., "Spatial Simulation of the Instability of Channel Flow with Local Suction/Blowing," *Physics of Fluids*, Vol. 9, No. 11, 1997, pp. 3258–3266.

[19]Pauley, L. R., Moin, P., and Reynolds, W. C., "The Structure of Two-Dimensional Separation," *Journal of Fluid Mechanics*, Vol. 220, 1990, pp. 397–411.

[20]Chung, Y. M., Sung, H. J., and Luo, K. H., "Response of Turbulent Channel Flow to Sudden Wall Suction and Blowing," *Advances in Turbulence VIII*, International Center for Numerical Methods in Engineering, Barcelona, 2000, pp. 109–112.

[21]Elena, M., "Suction Effects on Turbulence Statistics in a Heated Pipe Flow," *Physics of Fluids*, Vol. 27, No. 4, 1984, pp. 861–866.

[22]Kuroda, N. N., Kasagi, N., and Hirata, M., "Direct Numerical Simulation of Turbulent Plane Couette-Poiseuille Flows: Effect of Mean Shear Rate on the Near-Wall Turbulence Structures," *Turbulence Shear Flows 9*, edited by F. Durst, N. Kasagi, B. E. Launder, F. W. Schmidt, K. Suzuki, and J. H. Whitelaw, Springer-Verlag, Berlin, 1995, pp. 241–257.

[23]Kim, J., Moin, P., and Moser, R., "Turbulent Statistics in Fully Developed Channel Flow at Low Reynolds Number," *Journal of Fluid Mechanics*, Vol. 177, 1987, pp. 133–166.

[24]Mansour, N. N., Kim, J., and Moin, P., "Reynolds-Stress and Dissipation-Rate Budgets in a Turbulent Channel Flow," *Journal of Fluid Mechanics*, Vol. 194, 1988, pp. 15–44.

P. Givi
Associate Editor